ELM suppression by boron powder injection and comparison with lithium powder injection on EAST

R. Maingi[1], J.S. Hu[2], Z. Sun[1], A. Diallo[1], K. Tritz[3], Y.Z. Qian[2], W. Xu[2], G.Z. Zuo[2], C.L. Li[2], M. Huang[2], Y. Ye[2], A. Bortolon[1], E.P. Gilson[1], R. Lunsford[1], D.K. Mansfield[1], A. Nagy[1], J.P. Qian[2], X.Z. Gong[2], and the EAST team

[1]*Princeton Plasma Physics Laboratory, Princeton, NJ, USA*
[2]*Institue of Plasma Physics, Chinese Academy of Sciences, Hefei, China*
[3]*Johns Hopkins University, Baltimore, MD, USA*

email: rmaingi@pppl.gov (corresponding author), hujs@ipp.ac.cn

Abstract

Type I edge-localized modes (ELMs) in the Experimental Advanced Superconducting Tokamak (EAST) were completely suppressed via boron powder injection into the X-point region of an upper-single null configuration over a wide range of operating conditions ($2.8 < P_{aux} < 7.5$ MW, $3.8\times10^{19} < n_e < 6\times10^{19}$ m^{-3}, RF-only and RF+NBI heating scenarios, both grad-B drift directions, and even He ion majority plasmas) [Z. Sun et al., 2020 *Phys. Rev. Lett.* submitted]. A window of edge B concentration for stable long pulse operation was identified: too low and ELMs return, too high and the discharge suffers radiative collapse. The injection of boron powder above the minimum for ELM suppression coincided with the occurrence of an edge harmonic oscillation detected in magnetics (both on the high-field side and low-field side), in AXUV diodes near the upper X-point, divertor D_α emission, and in a range of other diagnostics [A. Diallo et al., "First Observation of ELM Suppression without Confinement Degradation due to Geodesic Acoustic Mode (GAM)-like mode Triggered by Boron Powder Injection", 2020 IAEA Fusion Energy Conference paper]. No harmonic oscillation was observed when ELMs were present, and stored energy was slightly increased at constant density during ELM suppression. Core tungsten emission during ELM suppression either increased or decreased relative to ELMy H-mode, but the W emission was maintained at acceptable levels. The threshold B injection rate was measured for several conditions, and found to increase with heating power. Li powder injection into comparable discharges also resulted in a short phase of ELM suppression, but density and stored energy both decreased due to the strong pumping effect of lithium; no edge harmonic oscillation was observed with Li injection, indicating that the ELM suppression mechanisms differ. The new set of B-seeded, ELM-suppressed discharges exhibited certain characteristics of quiescent H-mode [K.H. Burrell et al., 2001 Phys. Plasmas **8**, 2153], but did not require high shear, counter beams, etc. The wide operating window and compatibility with RF-only discharges paves the way for future experiments targeting long pulse H-mode discharges with complete ELM suppression.

Introduction and Experiment Setup

Impurities are injected into magnetic fusion devices to improve plasma performance in several ways. Until recently, impurities were injected in gaseous form, with a few isolated experiments using doped pellets, because robust control of solid impurity injection is difficult. Recently, a new device to gravitationally inject a wide range of impurity powders was developed[1]; this paper describes the use of this impurity powder dropper (IPD) to inject boron powder and eliminate edge-localized modes (ELMs) in the Experimental Advanced Superconducting Tokamak (EAST)[2], over a wide range of heating powers, line-average densities, and even in discharges with dominant helium majority plasma species.

The first-generation impurity injector of this type dropped spherical, metallic impurities onto a vibrating piezoelectric disk driven at resonant frequencies[3]. The impurities, usually lithium (Li), were accelerated via gravity through a hole in the center of the disk into a drop tube and into the boundary plasma. This dropper was first used on the National Spherical Torus Experiment (NSTX) to eliminate ELMs and improve energy confinement[3], similar to observations made with pre-discharge Li evaporation onto NSTX carbon plasma-facing components (PFCs)[4-6]. This type of a dropper injecting Li powder also eliminated ELMs on EAST, both with dominant carbon (lower divertor)[7] and tungsten (upper divertor)[8] PFCs. Although this dropper design was robust with excellent reproducibility, the desire to inject aspherically-shaped compounds with high granular friction ("stickiness"), e.g. boron-based compounds, necessitated a design change.

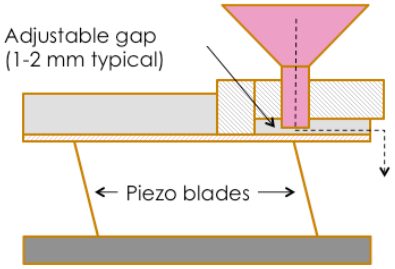

Figure 1: Schematic of single-channel impurity powder dropper. Present deployments use four channels 90° apart and a common drop tube[1].

The new generation impurity injector, developed over the last 3 years, uses vertically-mounted piezoelectric crystals for a horizontal drive off the edge of a surface into a drop tube (Figure 1), and is compatible with a wide range of impurity species, e.g. B, BN, B_4C, Li, Al, Si etc. and multiple sizes[1]. The lateral back-and-forth motion of up to 10 mm allows reproducible and calibratable impurity injection rates. An accelerometer and an optical sensor measure the injection rates, which are optimized in the 1-200 mg/s range optimal for low-Z impurities in present devices. This new dropper is also capable of injecting large particle sizes, e.g., up 10 mm diameter granules, into plasma discharges. The latest deployments feature four independent drop units using a common drop tube; weights have been added to each unit to achieve distinct resonant frequencies to minimize unintentional injection of impurities from the other three units when only one unit is activated. Versions of these droppers have also been implemented on the ASDEX-Upgrade[9, 10], DIII-D[11], KSTAR[12], and LHD devices, and a related concept was deployed on the W7-X device[13].

A picture of the four-chamber IPD is shown in Figure 2, along with the powder species and sizes used in EAST and the reconstructed plasma equilibrium shape. For this experiment, the high-purity B powder size of ~70 μm was used, along with ~50 μm Li powder used for comparison discharges. The IPD injected, i.e. dropped, vertically downward into the X-point region of upper-single null configurations in EAST (R=1.57m). For completeness, we also show where the classical Li powder dropper injected in previous experiments: on the low-field side radially outboard of the X-point (R=1.95m)[8, 14].

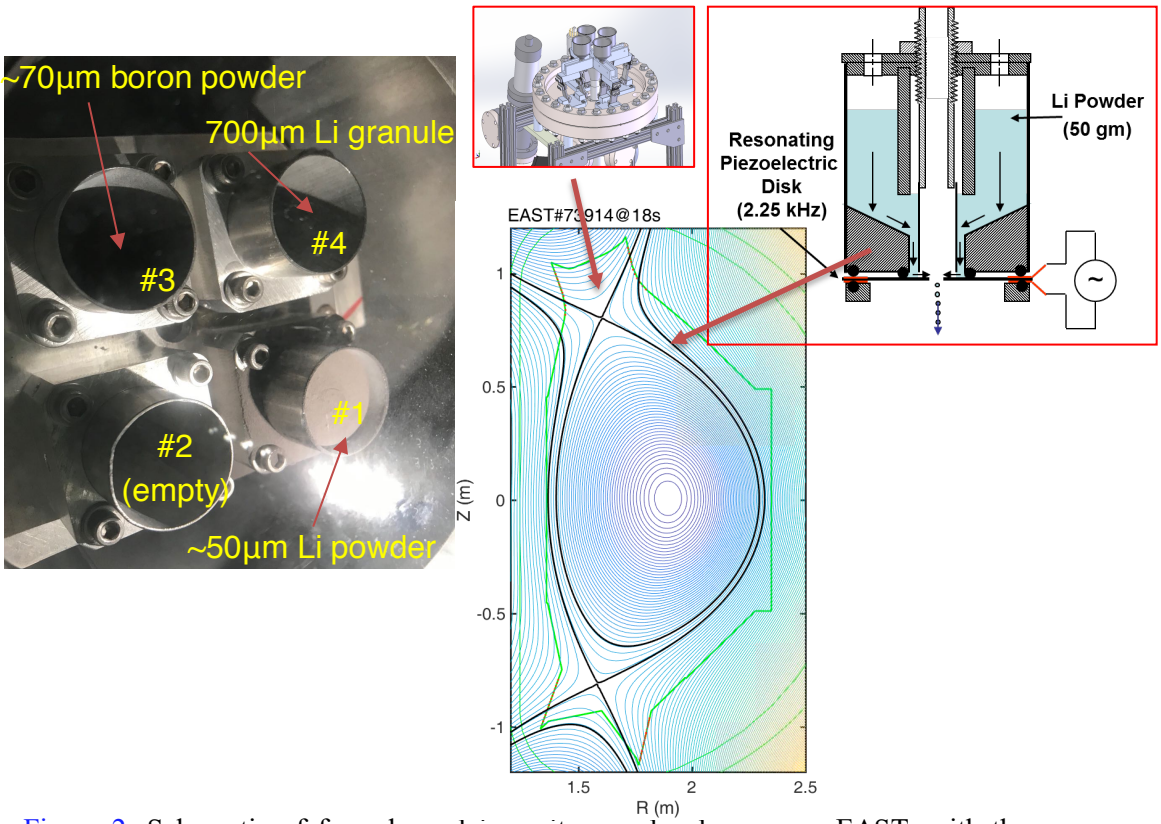

Figure 2: Schematic of four-channel impurity powder dropper on EAST, with the species loaded in each channel identified. The impurity powder dropper is located above the upper X-point, whereas the classical lithium dropper, with a single channel, is located outboard of the upper X-point.

Observation of ELM suppression with B powder injection

Robust ELM suppression was observed when sufficient B powder was injected above the upper X-point in upper-single null discharges[15]. A comparison of two discharges, one with B powder injection and ELMs suppressed, and one without B powder injection and ordinary Type I ELMs, is shown in Figure 3. The plasma current, heating power and mix were matched (panels 3a, 3c, 3d). The line-average density was matched (panel 3b) by moderately reducing the feed-forward gas puffing to counteract the electron fueling from B powder injection. B injection was initiated at about 1.7 s, and led to B-V emission from the plasma (panel 3f, red curve). The ELMs, visible as spikes in the upper divertor D_α emission in the reference discharge, were completely eliminated with B injection (panel 3g). ELMs typically result in a $\dot{B}$ perturbation; these were also eliminated in the B injection discharge (panel 3h). The plasma stored energy was modestly higher in the discharge without ELMs (panel 3i). The core O-VIII impurity was reduced, while the core W emission increased, but was held steady at an acceptable level (panel 3j). An interesting observation was that a vertical oscillation, manifest in e.g. the magnetic balance parameter d_{RSep}, was eliminated (panel 3e); we speculate that this happened because the ELMs present in the reference discharge initiated an oscillatory behavior. With ELMs suppressed, the vertical oscillation was eliminated. This last observation was robust: ELM suppression with B powder

injection in other discharges usually also suppressed the mid-discharge vertical oscillation that sometimes occurred.

Concomitant with the ELM elimination was destabilization of an edge-localized oscillation[16]. This oscillation has a principal frequency ~ 2-4 kHz, with multiple harmonics observable on Mirnov probes, AXUV diodes that measure radiated power, divertor D_α emission, beam-emission spectroscopy, interferometer, divertor Langmuir probes, etc. These fluctuations were observed on signals both inside and outside the separatrix, suggesting that the mode transports particles from the closed to open field lines. This transport is likely responsible for preventing impurity accumulation that occurs when ELM suppression is not accompanied by additional particle transport.

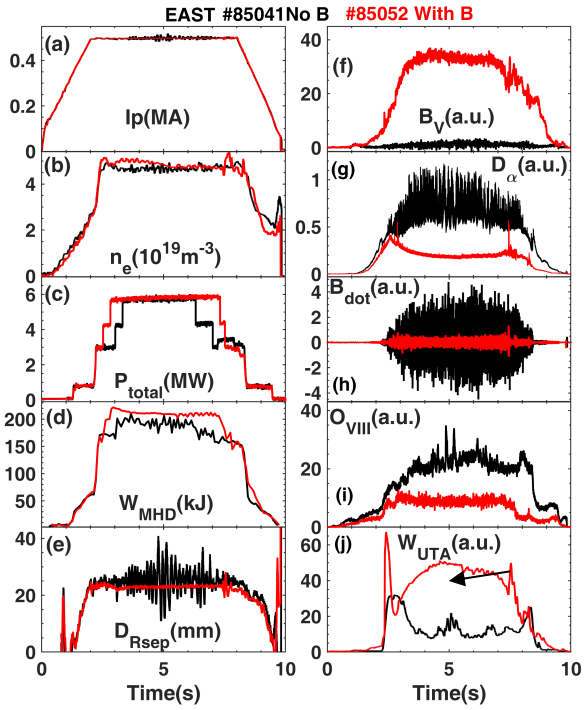

Figure 3: comparison of various quantities for a discharge with B powder injection (red) and one without (black): (a) plasma current I_p, (b) line-average electron density n_{eL}, (c) total heating power, (d) plasma stored energy W_{MHD}, (e) magnetic balance parameter d_{RSep}, (f) boron-V emission from edge plasma, (g) upper divertor D_α emission, (h) pickup from magnetic probe $\dot{B}$, (i) core O-VIII, and (j) and core W emission W_{UTA}.

An example of this oscillation is shown from AXUV diode signals in Figure 4. The lowest frequency of the mode in this discharge is ~ 3 kHz, with 2-3 harmonics observable. The mode is observable in all of the channels that look in the vicinity of the X-point, namely channels 52-59. The reason why these channels show the fluctuation is that the powder supplied a local electron source in the

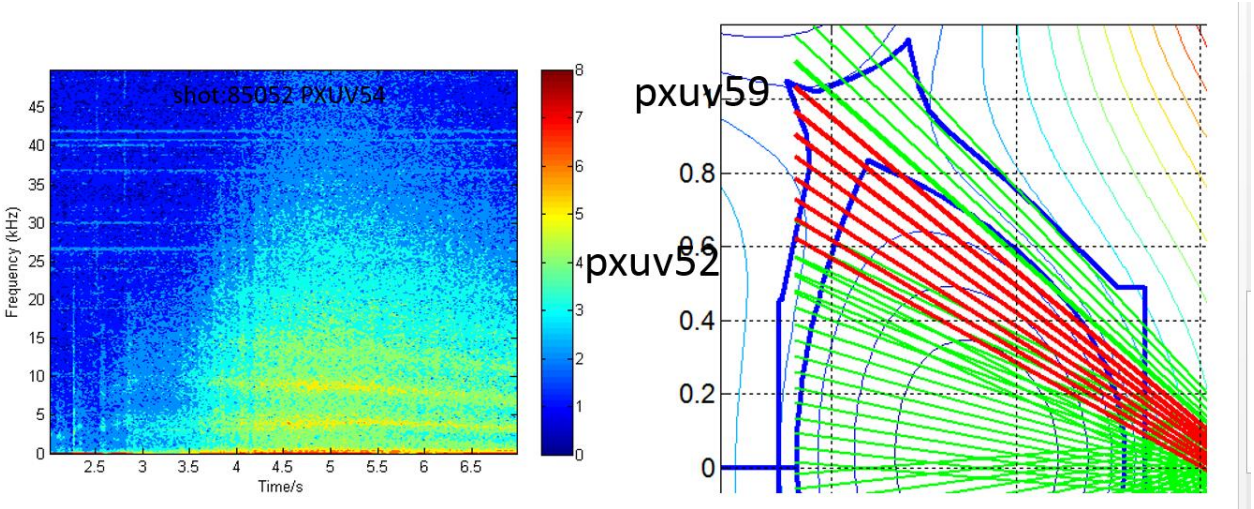

Figure 4: Left panel: observation of an edge mode with multiple harmonics observed in the radiated power measurements from AXUV diodes. The mode can be observed in channels 52-59, which are overlaid on an upper-single null equilibrium (right panel).

X-point region, which enhances the signal-to-noise ratio, improving contrast. Nonetheless, the mode is observed on many other diagnostics. The mode appears after ELMs are eliminated, once B in the edge plasma exceeds a critical threshold, which correlates with a particular level of B-V emission. The mode disappears when ELMs resume. B injection timing scans confirm causality: once the B edge emission falls below a threshold, ELMs re-appear, typically within 0.5 s of injection termination[15, 16].

The observation of ELM suppression with B injection is very robust in EAST. ELMs were suppressed by B injection over a range of auxiliary heating power (2.8 – 7.5 MW), with RF heating alone, with RF + NBI heating, over a range in line-average density ($3.7\text{-}6\times10^{19}$ m^{-3}), with ion grad-B drift toward and away from the upper X-point, and even in plasmas that use majority He fueling.

An example of ELM suppression in a discharge with ~ 70% He content is shown in Figure 5. The discharge in red has B injection and ELMs suppressed, whereas the discharge in black has no B injection and regular ELMs. The plasma current, line-density, heating power, and stored energy are all relatively well-matched (panels 3a, 3b, 3g, 3j). The feed-forward deuterium gas puffing rate was reduced in the discharge with B injection to balance the extra electron source with B (panel 3c). The He gas puffing was matched (panel 3d). The tungsten core impurity emission was modestly higher, possibly due to higher sputtering of W from the injected B (panel 3e). The B was injected at ~ 1.5 s, as seen in the elevated B-V emission (panel 3f). The spikes in visible light emission due to ELMs are eliminated (panels 3h, 3i). For completeness we note that the reason for seeding the plasma with 30% D content was to ensure a sufficiently low L-H power threshold to enable H-mode access with ~ 3 MW RF power (these discharges occurred shortly after a leak which left EAST with sub-optimal wall conditions).

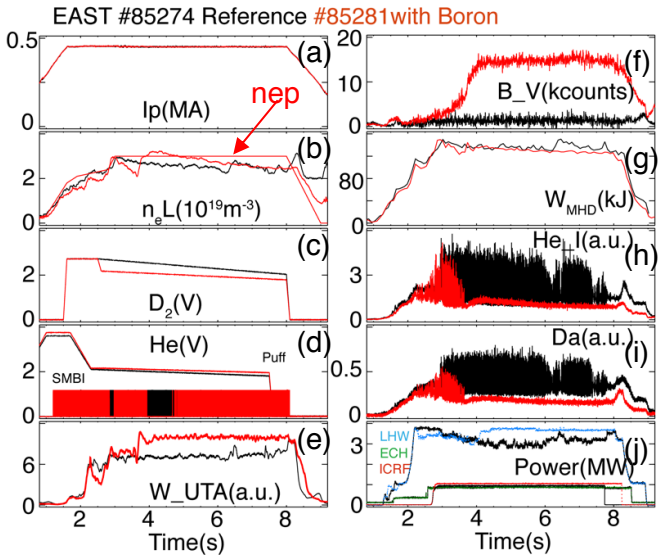

Figure 5: comparison of quantities for a discharge with B powder injection (red) and one without (black) for a discharge with 70% He content and 30% D content: (a) plasma current I_p, (b) line-average electron density n_{eL}, along with programmed density level, nep (c) deuterium gas puffing voltage from fueling valve, (d) helium gas puffing voltage from fueling valve, (e) core W emission W_{UTA}, (f) boron-V emission from edge plasma, (g) plasma stored energy W_{MHD}, (h) upper divertor He-1 emission (i) upper divertor D_α emission, and (j) heating from lower hybrid waves (LHW), electron cyclotron heating (ECH), and ion cyclotron radio frequency (ICRF) in MW.

Measurement of threshold B injection rate to suppress ELMs

An important element to evaluate the applicability of B powder injection for future, high power discharges is the minimum required injection amount/rate needed for ELM suppression, and its dependence on heating power. The actual threshold is a B edge concentration threshold, for which the B-V edge emission signal can be used as a good proxy. The threshold B-V emission level for

ELM suppression varies with electron density, heating power etc. Practically, it is important to characterize the needed B injection rate to achieve the threshold level for ELM suppression; this rate is expected to increase with heating power because B powder penetration through the scrape-off layer into the main chamber is less effective with increasing plasma density and temperature.

In practice, the minimum B powder injection rate to achieve complete ELM suppression can be measured with the present IPD, which has enough dynamic range and control to enable such a measurement. Figure 6 compares three discharges heated with RF-only power at 3.1 MW, all using 70 μm size B powder. The reference discharge without B injection is ELMy (blue curve). B injection was added from about 4-6.5 s, to leave a period of ELMs before B injection and after B concentration fell below the minimum level for ELMs to resume. The red curve (2 mg/s, 1.1 $\times 10^{20}$ atoms/s) shows elimination of many, but not quite all of the ELMs. The yellow curve with marginally higher injection (2.5 mg/s, 1.4×10^{20} atoms/s) shows elimination of all of the ELMs, and resumption of ELMs at the end of the discharge. All of the flow rates below 1.1×10^{20} atoms/s showed ELM mitigation but not suppression, while all of the flow rates above 1.4×10^{20} atoms/s resulted in complete ELM suppression. Empirically, there is an upper limit to B injection: if the flow rate is too high (usually 30-

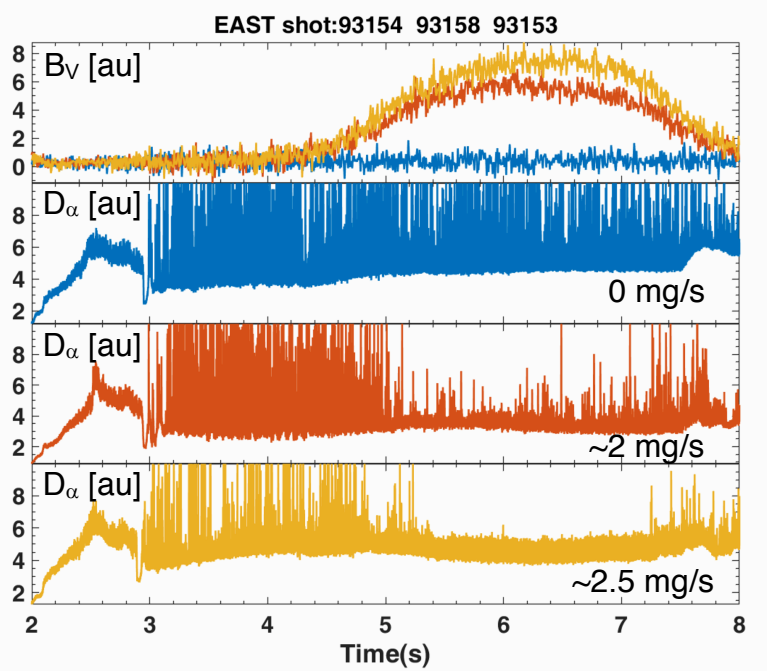

Figure 6: B powder injection rate scan for RF-only heated discharges with 3.1 MW auxiliary heating power, showing B-V emission from the edge and upper divertor D_α emission for 3 discharges. A threshold flow rate to eliminate ELMs was found between 2 and 2.5 mg/s (1.1e20 – 1.4e20 atoms/s).

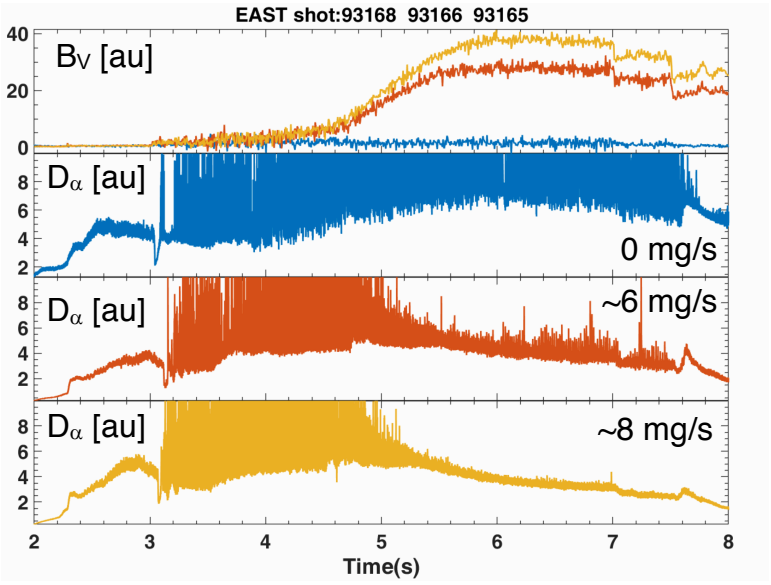

Figure 7: B powder injection rate scan for RF and NBI heated discharges with 6.1 MW auxiliary heating power, showing B-V emission from the edge and upper divertor D_α emission for 3 discharges. A threshold flow rate to eliminate ELMs was found between 6 and 8 mg/s (3.3e20 – 4.4e20 atoms/s).

40x above the threshold needed for suppression), enhanced radiation from B injected into the core triggers a core radiative collapse.

The experiment protocol was repeated for a sequence of discharges with twice as high auxiliary heating power of ~ 6.1 MW. Figure 7 shows the comparable set of discharges to Figure 6, but with the higher heating power, all using 70 μm size B powder from 4-6.5 s. It can be seen that ELMs are mitigated at a flow rate of 3.3×10^{20} atoms/s, and completely suppressed at 4.4×10^{20} atoms/s. Note also that the B-V emission signal needed for complete ELM suppression increases with heating power (compare the top panels in Figure 7 and Figure 6). Note that a doubling of the heating power (3 → 6 MW) resulted in a 3x higher B flow rate for ELM suppression, indicating that the minimum B injection rate increases faster than linearly with auxiliary heating power.

Comparison between ELM suppression with B injection and Li injection

The discharges used to study ELM suppression with B powder injection were repeated with Li powder injection using the IPD, to provide a direct comparison. Figure 8 compares two such discharges: with B powder (red) and Li powder (blue). The Li powder was injected continuously during the discharge (panel 8a), resulting in a slowly declining stored energy (panel 8b), and slowly declining recycling as indicated by the strong secular reduction in baseline divertor D_α emission (panel 8e). In contrast, the B was injected only from 1.7 s to 4 s, to demonstrate the resumption of ELMs shortly after termination of the B injection. Note that the W in the core was reduced with B injection in this case, whereas it increased with Li injection (panel 8c). The stored energy and D_α baseline emission remained high during the ELM-stable phase with B injection. This, coupled with other observations, suggests that recycling reduction *does not play a major role* in ELM suppression with B injection, which differs from the hypothesis for ELM suppression with Li injection: that reduced recycling leads to density and pressure profile changes that stabilize ELMs[17, 18]. In the case of B injection, the edge harmonic oscillation itself seems to be the key component for ELM suppression.

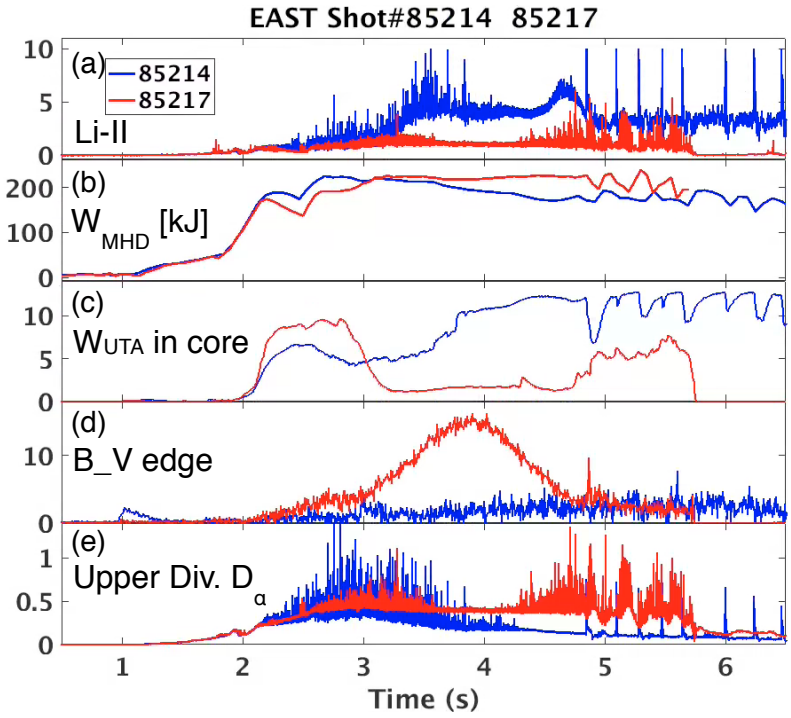

Figure 8: comparison of a discharge with B powder injection (red) and one Li powder injection (blue): (a) Li-II emission, plasma current I_p, (b) plasma stored energy W_{MHD}, (c) core W emission W_{UTA}, (d) boron-V emission from edge plasma, (e) and upper divertor D_α emission. The discharges had matched heating power and comparable density within ~ 10-15%.

Summary and Conclusions

We report robust ELM suppression over a wide range of operating conditions in EAST. The operational window for ELM suppression with B injection is wide in terms of heating power (both the level and mix of RF/ECH/NBI techniques), electron density, grad-B field direction, and even majority ion species (D and He). The minimum B injection rate to achieve ELM suppression was observed to increase non-linearly with heating power. For future reactors, this would result in a prohibitively high required flow rate if gravitational droppers, with relatively modest penetration into the scrape-off later plasma, are used. However, injecting the powder with a high speed rotary motor, as used for the lithium granule injector[19, 20] , would reduce the required material throughput, due to the higher radial injection velocities of 100-200 m/s that can be achieved with such systems. While these granule injectors are currently used for ELM mitigation via ELM pacing[21-23], careful selection of the granule size and velocity can be used to ensure penetration to just inside the separatrix, to maximize deposition inside the separatrix but not to the steep gradient region or pedestal top, which would result in ELM triggering[24, 25].

While the mechanism for ELM suppression by B injection is still under investigation, it does not appear to be tied to reduced recycling, as is the case for Li-induced ELM suppression. Rather, the triggered edge harmonic oscillation appears to be the key element to assure sufficient edge transport to avoid hitting the peeling-ballooning limit that destabilizes ELMs[26]. Consequently, present analysis is focusing on identifying the mode characteristics and onset conditions, to unravel the instability and its drive mechanisms.

At a high level, this operational scenario shares certain similarities with the quiescent H-mode[27], which requires strong rotation and electric field shear and low collisionality for access[28-30]. However, the scenario presented in this paper has a wider operating window, including full compatibility with torque-less RF heating scenarios, and over a wide collisionality range than QH-mode. Present work is focusing on conclusively identifying the ELM suppression mechanisms and making initial attempts to project extrapolability to future devices.

Acknowledgement: This research was supported in part by the U.S. Dept. of Energy Contracts DE-AC02-09CH11466, DE-FG02-09ER55012 and DE-FC02-04ER54698, and partly the by National Key Research and Development Program of China (2017YFA0402500 and 2017YFE0301100), and the National Nature Science Foundation of China (11625524, 11775261, 11605246). We gratefully acknowledge the contributions from the EAST technical staff.

References:

1. A. Nagy *et al.*, 2018 *Rev. Sci. Instrum.* **89** 10K121
2. B. Wan *et al.*, 2015 *Nucl. Fusion* **55** 104015
3. D. K. Mansfield *et al.*, 2010 *Fusion Eng. Des.* **85** 890
4. H. W. Kugel *et al.*, 2008 *Phys. Plasmas* **15** 056118
5. M. G. Bell *et al.*, 2009 *Plasma Phys. Control. Fusion* **51** 124054
6. R. Maingi *et al.*, 2012 *Nucl. Fusion* **52** 083001
7. J. S. Hu *et al.*, 2015 *Phys. Rev. Lett.* **114** 055001
8. R. Maingi *et al.*, 2018 *Nucl. Fusion* **58** 024003
9. A. Bortolon *et al.*, 2019 *Nucl. Mater. Energy* **19** 384
10. R. Lunsford *et al.*, 2019 *Nucl. Fusion* **59** 126034
11. A. Bortolon, 2020 *Phys. Plasmas* submitted
12. E. P. Gilson *et al.*, 2019 *submitted to 2019 EPS conference*
13. A. Nagy *et al.*, 2019 *Fusion Eng. Des.* **146** 1403
14. Z. Sun *et al.*, 2019 *Nucl. Mater. Energy* **19** 124
15. Z. Sun *et al.*, 2020 *Phys. Rev. Lett.* subm
16. A. Diallo, 2020 *Proc. 2020 IAEA Fusion Energy Conference, Nice, France, 12-17 Oct. 2020* subm.
17. R. Maingi *et al.*, 2009 *Phys. Rev. Lett.* **103** 075001
18. J. M. Canik *et al.*, 2011 *Phys. Plasmas* **18** 056118
19. D. K. Mansfield *et al.*, 2013 *Nucl. Fusion* **53** 113023
20. A. Bortolon *et al.*, 2016 *Nucl. Fusion* **56** 056008
21. R. Lunsford *et al.*, 2018 *Nucl. Fusion* **58** 126021
22. Z. Sun *et al.*, 2018 *IEEE Trans. Plasma Sci.* **46** 1076
23. R. Lunsford *et al.*, 2018 *Nucl. Fusion* **58** 036007
24. G. Huysmans, S. Pamela, E. van der Plas, and P. Ramet, 2009 *Plasma Phys. Control. Fusion* **51** 124012
25. L. R. Baylor *et al.*, 2013 *Phys. Rev. Lett.* **110** 245001
26. P. B. Snyder *et al.*, 2002 *Phys. Plasmas* **9** 2037
27. K. H. Burrell *et al.*, 2001 *Phys. Plasmas* **8** 2153
28. A. M. Garofalo *et al.*, 2011 *Nucl. Fusion* **51** 083018
29. X. Chen *et al.*, 2016 *Nucl. Fusion* **56**
30. T. M. Wilks *et al.*, 2018 *Nucl. Fusion* **58**